energies

MDPI

Article

Process Simulation of a Temperature Swing Absorption Process for Hydrogen Isotope Separation

Annika Uihlein *, Jonas Caspar Schwenzer, Stefan Hanke and Thomas Giegerich *

Institute for Technical Physics (ITEP), Karlsruhe Institute of Technology (KIT), 76131 Karlsruhe, Germany
* Correspondence: annika.uihlein@kit.edu (A.U.); thomas.giegerich@kit.edu (T.G.)

Abstract

Temperature Swing Absorption (TSA) is the primary candidate for the Isotope Rebalancing and Protium Removal (IRPR) system within the envisioned EU-DEMO fusion reactor fuel cycle. TSA separates a mixed hydrogen isotope stream into two product streams using a semi-continuous process. One stream, enriched in heavy isotopes, is used to re-establish the required deuterium-to-tritium fuel ratio. The second, enriched in protium, is stripped off from the fuel cycle to counteract the protium build-up. Separation is achieved by cycling an isotope mixture between two columns filled with metallic absorption materials that have opposite isotope effects of metal hydride formation. The selection of these materials, the operation parameters and the column geometry allow for adjusting the resulting enrichments. To identify suitable operation parameters, a TSA process model is developed which depicts the process dynamics and interactions between the columns. A modified process operation mode is introduced, which enables higher system throughputs and non-cryogenic operation, i.e., operational temperatures between 0 to 130 °C, while reducing the tritium inventory due to shorter cycling times by reduced amplitudes of the temperature swings. Finally, simulations of a TSA system at relevant scale confirm the suitability of TSA technology for the separation task of the EU-DEMO IRPR system.

Keywords: process model for hydrogen isotope separation; fuel cycle; metal-hydrogen interactions; Temperature Swing Absorption

1. Introduction

In the fuel cycle of the envisioned EU-DEMO fusion reactor, the Isotope Rebalancing and Protium Removal (IRPR) unit provides a hydrogen isotope separation function that establishes the specified deuterium-to-tritium ratio and counteracts the built-up of protium within the recycled fuel stream [1]. Protium enters the fuel due to outgassing from the torus vacuum chamber and accumulates over time since it is not burnt during the fusion reaction. Furthermore, protium contents above 1% may lead to plasma instabilities. The IRPR system is placed downstream of the torus within the inner loop of the EU-DEMO fuel cycle and is fed with a stream of hydrogen isotopes from the exhaust processing system. A Temperature Swing Absorption (TSA) process was selected as the primary technology for the IRPR system due to its promising ability to operate semi-continuously with low tritium inventories at moderate operation parameters and reduced energy consumption in comparison to cryogenic distillation technology [2,3].

The TSA process exploits isotope-dependent metal–hydrogen interactions to achieve their separation. Certain metals or alloys show an isotope effect when forming their corresponding hydride, which is expressed by the separation factor. A well-investigated

Academic Editor: Alberto Pettinau

Received: 18 November 2025
Revised: 9 January 2026
Accepted: 14 January 2026
Published: 17 January 2026

metal for this is palladium, which has a higher affinity to absorb and react with lighter hydrogen isotopes [4,5]. To utilize this effect within a process for isotope separation, isotopic-sensitive metals are filled in absorption columns. Introducing an isotope mixture into such a column leads to an accumulation of the favored isotope(s) species in the absorbent. This separation can be further intensified by allowing the isotope mixture to flow through the packed column. This causes, besides the thermodynamic equilibrium-based separation (single-stage), a chromatographic separation effect (multi-stage).

A well-established TSA process for the separation of binary isotope mixtures is the TCAP (Thermal Cycling Absorption Process) developed by Savannah River National Laboratories. In this process, palladium coated on inert kieselguhr or alumina oxide is the absorption material. Different development stages of the process are published in the literature [6–9]. While the original TCAP utilizes an inert non-separating plug flow reverser (PFR) column filled with kieselguhr as a second column, in an improved process, a molecular sieve is used [3,10]. This has the advantage of showing an opposite isotopic effect compared to the palladium column, hence contributing to the isotope separation and doubling the process throughput [10]. Recently, benchmarking tests to evaluate the separation performance of single packed columns and molecular sieves were reported to identify design parameters for optimization [11]. However, major drawbacks of using a molecular sieve as second column are the required cryogenic operation temperatures. Until now, TCAP solutions have not been able to satisfy the presented IRPR requirements, because of high tritium inventories, cryogenic process temperatures and limited system throughput.

To overcome these challenges, an optimized TSA process with a second active separation column has been developed at KIT [2,12]. The novel approach herein is to replace the inert PFR or molecular sieve with a column filled with a metallic absorption material that shows an opposite isotope effect to the other, palladium-filled column. In this second column, the heavy isotopes are absorbed preferably. A schematic comparison of (traditional) TCAP (a) and the presented optimized TSA process (b) is shown in Figure 1. A general process description of TCAP is presented in detail in [6,13], while the process routine for the optimized TSA process is detailed in [12] accordingly. A low-pressure hydrogen storage material based on a titan–manganese alloy was developed and investigated for the optimized TSA process. It proved to be a promising absorption material to be paired with palladium. The main advantage of utilizing two interacting active separation columns is the pumping effect provided by the materials during absorption. By this, the column in the absorption phase enhances the withdrawal of isotopes from the column in the desorption phase. This allows for lower desorption and higher absorption temperatures. Coupling those two absorption materials allows for process operation above 0 °C, setting it apart from TCAP solutions that use a molecular sieve. Besides the expected reduction of energy consumption due to the lowered amplitude of the temperature swings and moderate temperature level, the time required for heating and cooling is also shorter, which reduces the total process cycle time. Furthermore, lower process pressures result and the tritium inventory decreases.

The simulation tool presented here supports the design of the TSA process. The scope of the model is chosen to simulate the dynamic process behavior under tritium operation. Simulation results shall deliver predictions for process characteristics such as an estimation of operation pressures and product compositions as a function of operation temperatures and design (column geometry, sorbent quantities). Using these results, the achievable systems throughput, residence times, and numbers of required parallel columns to fulfill the separation tasks can be computed. Ultimately, it also allows for the verification of the stability of operational points fulfilling the EU-DEMO IRPR requirements. The simulation tool is rather simple and robust, and, as needed at this early design stage,

allows for rapid design iterations to evaluate process feasibility. The developed model is based on differential matter and energy conservation equations and is comparable to reported TSA models [14–18]. While Zhou et al. developed a CFD model to describe the separation efficiency of a palladium column coupled with a molecular sieve [17], Robinson et al. evaluated the effectiveness of two combined palladium columns towards the separation efficiency [16]. In contrast, the TSA model presented here is extended by the implementation of a second active separation column filled with an inverse absorption material and allows for simulating the dynamic interaction between both packed columns. To establish a trustworthy simulation tool, physical rate-based model approaches are used. The required model parameters are extracted from experimental results or by experimental experience. Hence, a versatile TSA simulation tool is presented that points out promising operation ranges for large-scale IRPR operation.

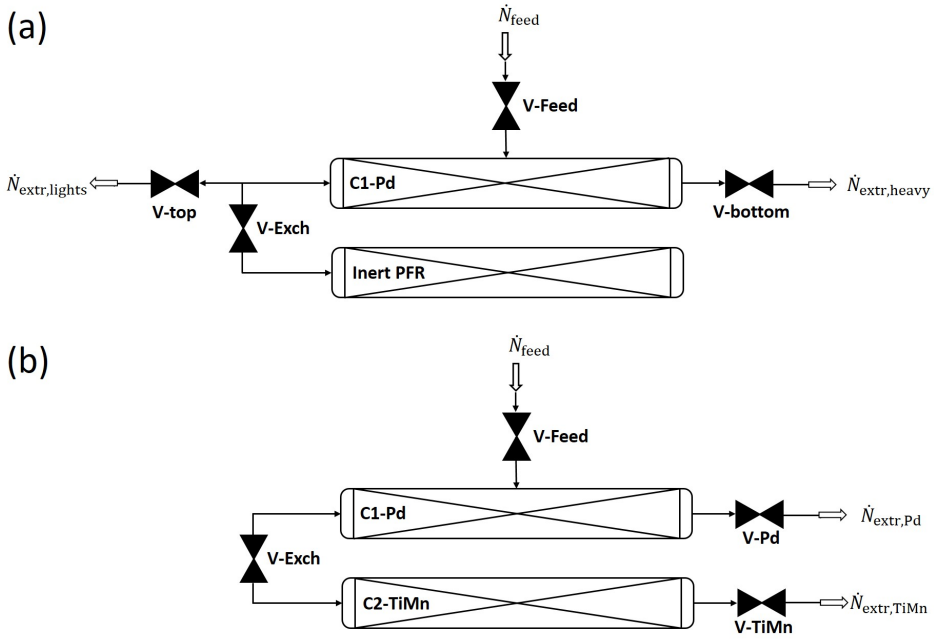

Figure 1. (**a**) Schematic description of TCAP in comparison to (**b**) optimized TSA process extended by a second active separation column C2.

First, the model set-up and the model equations are presented in Section 2. For this, the model is categorized into sub-models. Additionally, the process operation schedule and its implementation are described. An alternative operation mode is introduced, exploiting the coupling of two metallic absorption materials, and its promising advantages are detailed. In Section 3, the presented model is used to run an example case, which verifies the assumptions made for the optimized TSA set-up and demonstrates the process utility for the EU-DEMO IRPR system.

2. Model Set-Up

The process model is implemented in the Aspen Custom Modeler flow sheet simulation software using 1D transient equation-based models. The time-dependent differential equations are solved by using the implicit Euler integration, while relative and absolute tolerances are set to 1×10^{-5}. The presented TSA model can easily be integrated within the overall fuel cycle simulator framework, which is developed at KIT using the same software [19]. The process model consists of two interacting absorption columns, namely the palladium and the titanium–manganese column (see Figure 1b). The interaction between both columns, as well as the two product extractions and the feed supply, is realized

using valve models, whose opening and closing actions are triggered in time following repeated automated process steps that reflect the dynamic process scheduling. The columns are discretized along their length axis in segments of length dx. A segment dx with all occurring model variables of gas and solid phase is shown in Figure 2.

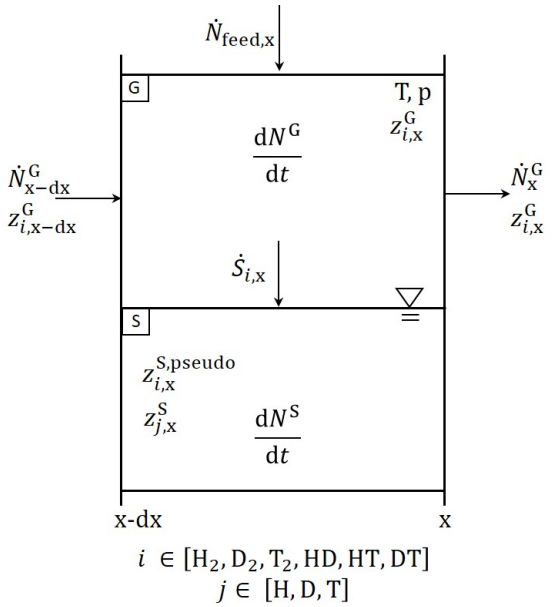

Figure 2. Column segment dx and the occurring molar streams between neighbor elements, solid and gas phase.

In the following, the balances and constitutive equations used in the model are presented. All utilized symbols and their units are summarized in the List of Symbols.

2.1. Description of Gas Phase

The gas phase in a column segment dx is modeled as a mixture of the six molecular hydrogen isotopologues Q_2: H_2, HD, D_2, DT, T_2 and HT. The change of the total molar amount in the gas phase N^{G} over time t, i.e., $\left(\frac{\partial N^{\mathrm{G}}}{\partial t}\right)_{\mathrm{x}}$, during the different process phases within the element dx is given by the material conservation balance

$$\left(\frac{\partial N^{\mathrm{G}}}{\partial t}\right)_{\mathrm{x}} = \dot{N}^{\mathrm{G}}_{\mathrm{x-dx}} - \dot{N}^{\mathrm{G}}_{\mathrm{x}} - \dot{S}^{\mathrm{G}}_{\mathrm{x}} + \dot{N}_{\mathrm{feed,x}}. \tag{1}$$

where $\dot{N}^{\mathrm{G}}_{\mathrm{x-dx}}$ and $\dot{N}^{\mathrm{G}}_{\mathrm{x}}$ represent the incoming and outgoing molar flows provided by neighbor elements, $\dot{N}_{\mathrm{feed,x}}$ is the molar feed stream and $\dot{S}^{\mathrm{G}}_{\mathrm{x}}$ is the molar flow transferred between the gas and solid phase due to absorption or desorption of the isotopologue molecules Q_2. Transport in the x-direction is assumed to be purely convective, hence any possible diffusive transport contribution is neglected. Similarly, the species balance for any of the isotopologues i follows by

$$\left(\frac{\partial N^{\mathrm{G}}_{i}}{\partial t}\right)_{\mathrm{x}} = \dot{N}^{\mathrm{G}}_{i,\mathrm{x-dx}} - \dot{N}^{\mathrm{G}}_{i,\mathrm{x}} - \dot{S}^{\mathrm{G}}_{i,\mathrm{x}} + \dot{N}_{i,\mathrm{feed,x}} \tag{2}$$

with the molar amount N^{G}_{i} of species i and the molar isotopic fractions $z^{\mathrm{G}}_{i,\mathrm{x}}$

$$z^{\mathrm{G}}_{i,\mathrm{x}} = \frac{N^{\mathrm{G}}_{i,\mathrm{x}}}{\sum_i N^{\mathrm{G}}_{i,\mathrm{x}}}, \tag{3}$$

where i = H_2, HD, D_2, DT, T_2 and HT.

The convective gas transport is implemented according to Darcy's law, as an estimation of the Reynolds number revealed a laminar flow regime through the packed column. The decrease of pressure p over the length is linear to the gas velocity u, the gas viscosity $\mu(T)$, the permeation parameter k and the cross-section A according to

$$\left(\frac{\mathrm{d}p}{\mathrm{d}x}\right)_{\mathrm{x}} = -\frac{\mu(T_{\mathrm{x}})}{k} u_{\mathrm{x}}. \tag{4}$$

u is replaced by the molar flow using the ideal gas law

$$u_{\mathrm{x}} = \frac{RT_{\mathrm{x}}}{p_{\mathrm{x}} A} \dot{N}_{\mathrm{x}}^{\mathrm{G}} \tag{5}$$

and a power law correlation is included to express the temperature dependence of μ

$$\mu(T_{\mathrm{x}}) = \mu^* \left(\frac{T_{\mathrm{x}}}{T^*}\right)^{0.668} \tag{6}$$

with the standard temperature T^* and standard viscosity $\mu^*(T^*)$. A combined transport parameter k_{p} is used to summarize the constant term $\frac{R\mu^*}{kAT^{*0.668}}$ and is determined by pressure drop measurements using a column mock-up, as described in the Appendix A.

To model the uptake and desorption rates represented by the transferred molar flow $\dot{S}_{i,\mathrm{x}}^{\mathrm{G}}$ of species i, a first-order rate approach is used

$$\dot{S}_{i,\mathrm{x}}^{\mathrm{G}} = k_{\mathrm{sorb},i}(T_{\mathrm{x}}) \left(p_{i,\mathrm{x}} - \mathtt{hys} \cdot p_{\mathrm{eq},i,\mathrm{x}}(z_{j,\mathrm{x}}^{\mathrm{S}}, c_{\mathrm{x}}, T_{\mathrm{x}})\right) \tag{7}$$

combined with Dalton's law

$$p_{i,\mathrm{x}} = z_{i,\mathrm{x}}^{\mathrm{G}} p_{\mathrm{x}}. \tag{8}$$

The driving force is given by the pressure difference to the equilibrium pressure $p_{\mathrm{eq},i,\mathrm{x}}(z_{j,\mathrm{x}}^{\mathrm{S}}, c_{\mathrm{x}}, T_{\mathrm{x}})$, valid for the system temperature and concentration and molar fraction of the atomic isotopes Q absorbed in the metal (c.f. Equations (17) and (18)). For partial pressures p_i greater than $p_{\mathrm{eq},i,\mathrm{x}}(z_{j,\mathrm{x}}^{\mathrm{S}}, c_{\mathrm{x}}, T_{\mathrm{x}})$ this results in absorption, while for lower partial pressures desorption takes place. The difference between the absorption and desorption isotherms is denoted as hysteresis, a phenomenon that results from stresses induced by hydrogenation and the resulting plastic and elastic deformation of the metal lattice [20]. It is respected by the hysteresis factor `hys`, which takes the value 1 for absorption and values <1 for desorption, depending on the characteristics of the utilized absorption material. The reaction coefficient $k_{\mathrm{sorb},i}$ can be derived from experimental sorption data.

Furthermore, in gas phases which contain different hydrogen isotopes, isotope exchange reactions occur. These are

$$H_2 + D_2 \rightleftharpoons 2\,HD \tag{9a}$$

$$D_2 + T_2 \rightleftharpoons 2\,DT \tag{9b}$$

$$H_2 + T_2 \rightleftharpoons 2\,HT \tag{9c}$$

A correlation for the corresponding temperature-dependent equilibrium constant $K_{jk,j\neq k,\mathrm{x}}$ for the given reactions is reported by Peters [21], based on data provided by Urey [22]:

$$K_{jk,j\neq k,\mathrm{x}} = A_{jk,j\neq k} \cdot \exp\left(-\frac{B_{jk,j\neq k}}{T_{\mathrm{x}}}\right). \tag{10}$$

The correlation parameters $A_{jk,j\neq k}$ and $B_{jk,j\neq k}$ for temperatures above 250 K are given in Table 1.

Table 1. Parameters of the temperature-dependent correlation of the equilibrium constant for each occurring isotope exchange reaction above 250 K [21].

Exchange Reaction	$A_{jk,j\neq k}$/-	$B_{jk,j\neq k}$/K
$H_2 + D_2 \rightleftharpoons 2\,HD$	4.075	19.456
$D_2 + T_2 \rightleftharpoons 2\,DT$	4.518	166.588
$H_2 + T_2 \rightleftharpoons 2\,HT$	4.207	75.316

While the impact of the isotope exchange reactions is neglected in the gas phase due to the low system temperatures and process times shorter than times necessary to reach the equilibrium composition, the described reactions are, however, used to model the composition of isotopes emerging from the metal during desorption, which is presented in Section 2.2.

2.2. Description of Solid Phase

In contrast to the gas phase, only three atomic isotope species Q: H, D and T exist in the solid phase, as a hydrogen isotope molecule dissociates on the metal surface $Me_{(S)}$ and forms a metal hydride $Me_aQ_{2b(S)}$ according to

$$aMe_{(S)} + bQ_{2(G)} \rightleftharpoons Me_aQ_{2b(S)} + \Delta H_r. \tag{11}$$

The accumulation of the sum of all Q-species $N^S = \sum_j N_j^S$, j = H, D, T is modeled by

$$\left(\frac{dN^S}{dt}\right)_x = \dot{S}_x^G. \tag{12}$$

Consequently, the species balance for atomic species j is written by

$$\left(\frac{dN_j^S}{dt}\right)_x = 2\dot{S}_{jj,x}^G + \dot{S}_{jk,j\neq k,x}^G + \dot{S}_{jl,j\neq l,x}^G, \tag{13}$$

where j, k, l = H, D, T and

$$z_{j,x}^S = \frac{N_{j,x}^S}{\sum_j N_{j,x}^S} \tag{14}$$

represents the atomic composition of the absorbed Q-species in the solid phase.

Equation (7) demands the implementation of six isotopologue-specific equilibrium pressures $p_{eq,i}(z_j^S, c, T)$ for molecular sorption kinetics. While the dependence of $p_{eq,i}(z_j^S, c, T)$ of the system temperature T is rather trivial, modeling the impact of the abundance of atomic species j in the metal lattice is challenging. Therefore, a pseudo-phase is introduced, which resembles a solid phase, but allows for molecular loading of Q_2 species in the lattice. In the broadest sense, this pseudo molecular transition phase can be physically interpreted as the metal surface, where Q_2 species dissociate and Q-species recombine. The composition of isotopologues in this pseudo-phase resembles the molecular composition representative for the atomically Q-loaded solid phase, and is influenced by the exchange with the gas (absorption) and solid phase (desorption), respectively. This enables us to model the establishing equilibrium pressure in the gas phase for isotopologue species i, weighted according to the abundance of atomic species j in the mixed solid phase. The molar composition $z_{j,x}^S$ of the solid phase for species j and the molar composition

$z_i^{\mathrm{S,pseudo}}$ of the pseudo-phase for species i are connected by the atomic balance of homo- and hetero-isotopologues according to

$$z_{j,\mathrm{x}}^{\mathrm{S}} = 2z_{jj,\mathrm{x}}^{\mathrm{S,pseudo}} + z_{jk,j\neq k,\mathrm{x}}^{\mathrm{S,pseudo}} + z_{jl,j\neq l,\mathrm{x}}^{\mathrm{S,pseudo}}. \tag{15}$$

The composition of isotopologues emerging from the pseudo solid phase is modeled by the equilibrium of the isotope exchange reactions given in Equation (9c).

$$K_{jk,j\neq k}(T_\mathrm{x}) = \frac{z_{jj,\mathrm{x}}^{\mathrm{S,pseudo}} \cdot z_{kk,\mathrm{x}}^{\mathrm{S,pseudo}}}{\left(z_{jk,j\neq k,\mathrm{x}}^{\mathrm{S,pseudo}}\right)^2}. \tag{16}$$

Here, the presence of exchange reactions comparable to a gas phase of mixed isotopes is assumed. The hypothesis of an equilibrium composition is justified by the metal serving as a catalyst and therefore accelerating the reaction until the equilibrium is reached, and was also exploited in [23].

The resulting isotopologue-specific equilibrium pressure $p_{\mathrm{eq},i,\mathrm{x}}$, depending on its abundance in the metal lattice, is calculated using Raoult's law, assuming ideal mixture behavior [24]

$$p_{\mathrm{eq},i,\mathrm{x}} = z_{i,\mathrm{x}}^{\mathrm{S,pseudo}} p_{\mathrm{eq,pseudo},i,\mathrm{x}}(z_i^{\mathrm{S,pseudo}} = 1, c_\mathrm{x}, T_\mathrm{x}). \tag{17}$$

$p_{\mathrm{eq,pseudo},i}(c_\mathrm{x}, T_\mathrm{x})$ reflects the establishing equilibrium pressure if only isotopologue species i was present in the solid phase, i.e., $z_i^{\mathrm{S,pseudo}} = 1$, and can be obtained from experimental pressure–concentration–isotherm (PCI) measurements. Beside on the system temperature T, the value of $p_{\mathrm{eq,pseudo},i}$ is dependent on the total number of moles N^{S} of absorbed isotope species Q in relation to the molar amount of the absorption material N_{mat}, which is expressed by the total concentration c of isotopes absorbed in the metal. This atomic loading is defined by

$$c_\mathrm{x} = \frac{N_\mathrm{x}^{\mathrm{S}}}{N_{\mathrm{mat},x}}. \tag{18}$$

2.3. Energy Balance

The energy balance for a column element dx is calculated by

$$\left(\frac{\mathrm{d}H}{\mathrm{d}t}\right)_\mathrm{x} = \dot{H}_{\mathrm{x-dx}} - \dot{H}_\mathrm{x} + \dot{Q}_\mathrm{x} + \dot{H}_{r,x}, \tag{19}$$

where H refers to the enthalpy. As a first approach and simplified description, axial convective heat transport in the gas phase is neglected, as well as axial heat conduction in the solid phase, i.e., $\dot{H}_{\mathrm{x-dx}} = \dot{H}_\mathrm{x} = 0$. $\dot{Q}_\mathrm{x}$ is the radial heat transfer provided by a heating system and $\dot{H}_r$ is the reaction enthalpy of hydride formation. Neglecting the heat capacity of the gas phase and summarizing the structure and absorption material densities in ρ^{S} Equation (19) can be rewritten to

$$\left(\frac{\mathrm{d}T}{\mathrm{d}t}\right)_\mathrm{x} = \frac{1}{\rho^{\mathrm{S}}\mathrm{d}xc_\mathrm{p}^{\mathrm{S}}}\left(\dot{Q}_\mathrm{x} + \Delta h_{\mathrm{sorb}}\dot{S}_{i,\mathrm{x}}^{\mathrm{G}}\right), \tag{20}$$

where Δh_{sorb} is the heat of absorption released during hydrogen uptake and $c_\mathrm{p}^{\mathrm{S}}$ is the isobaric heat capacity of the column. The thermal kinetic follows from

$$\dot{Q}_\mathrm{x} = k_{\mathrm{heat}}\pi D_{\mathrm{col}}\mathrm{d}x(T_{\mathrm{oil}} - T_\mathrm{x}), \tag{21}$$

where k_{heat} depicts the heat transmittance from the thermofluid (e.g., oil) through the wall of the column of diameter D_{col} to the absorbent. It is assumed that the flow rate and the used mass of the thermofluid are such that no temperature variations of the oil T_{oil} over time and column length occur:

$$\frac{dT_{oil}}{dt} = \frac{dT_{oil}}{dx} = 0. \tag{22}$$

It should be noted that the shown implementation of the energy balance to model the temperature changes within the column is a simple first approach that can be further extended to a model, taking into account the temperature dynamics of the thermofluid if found to be necessary. However, the engineering design of the temperature cycling system should be sufficient to provide close to ideal heating and is expected not to affect the evaluation of the general process efficiency.

2.4. Process Control and Boundaries

To model and monitor the process cycling steps, time-triggered valve models are used. They enable the exchange between the separation columns, the extraction of enriched product fractions and the feed supply. For extraction valves and feed valves, the molar flow $\dot{N}^G$ is set as a boundary condition as

$$\dot{N}^G = \begin{cases} 0, & \text{Closed valve,} \\ \texttt{fixed value}, & \text{Open valve.} \end{cases} \tag{23}$$

and equals a sample extraction by a mass flow controller. The composition of isotopes and temperature equals the values calculated in the neighbor columns element connected to the valve. The process step times for those open cycles (process steps that allow matter transfer over the system boundary) are based on preliminary tests and assumptions.

The exchange valve model differs to that of Equation (23), as a flow can occur in both directions between the columns, depending on the current pressure difference. The transferred molar stream is therefore modeled using a linear pressure–flow correlation, where k_{CV} represents a flow coefficient and the pressure difference $(p_{C1} - p_{C2})$ between the columns C1 and C2, defining the transport direction as follows:

$$\dot{N}^G = \begin{cases} 0, & \text{Closed valve,} \\ k_{CV}(p_{C1} - p_{C2}), & \text{Open valve.} \end{cases} \tag{24}$$

Additionally to the process step-dependent opening actions of the mentioned valves, the temperature of the thermofluid T_{oil} is set as a boundary condition:

$$T_{oil} = \begin{cases} T_{hot}, & \text{Heating,} \\ T_{cold}, & \text{Cooling.} \end{cases} \tag{25}$$

For each column an absorption temperature T_{cold} and a desorption temperature T_{hot} are implemented, which serve as the driving force for the thermal kinetic given in Equation (21).

2.5. Parameter Sensitivity

Several operational parameters have an impact on the separation efficiency of the proposed TSA process. In general, operational, particle and design parameters influencing the separation efficiency as reported for traditional and advanced TCAP systems are also valid for the presented TSA process herein. Beside the recent report by Savannah River National Laboratories towards the impact of the particle diameter, the bed temperature and

the flow rate on the resulting number of separation stages [11], model parameter studies concerning the feeding ratio, the feed position, the reflux ratio and the selected operational temperatures can be found [17,18]. Therefore, a very brief description of the impact of two coefficients for the TSA model presented here is given, which can be concluded from the respective model equations.

Transport coefficient k_p: This specific model parameter appears in the transport kinetic term (c.f. Equation (4)) and is obtained by flow through experiments (c.f. Appendix A). A linear dependency between k_p and the gas velocity exists, which in turn impacts the establishing number of separation stages within the packed column. The parameter has to be adapted for each column packing respectively, since it is defined by the particle diameter and the bed porosity. The complex dependency of the gas transport on those bed parameters and the resulting separation efficiency motivated the studies in [11].

Heat coefficient k_{heat}: The implemented heat coefficient k_{heat} determines the heat transmittance from the heating or cooling media through the wall of the column. A linear dependency exists between the transferred radial heat flow $\dot{Q}$ and k_{heat}, according to Equation (21). Introducing this kinetic approach in Equation (20) and assuming the provided heat by the heating system to be dominant over the released heat of absorption, i.e., $\dot{Q} \gg \Delta h_{sorb} \dot{S}^G$, a reciprocal correlation between the required heating time and k_{heat} is obtained. The maximization of the heat transfer of a TSA set-up is envisioned, as the high-level consequence is a reduced overall cycling time and thus an increased process throughput.

2.6. Process Schedule Variants

Two process variants are described in the following.

Variant A: A typical sequence of a complete TSA cycle is given in Table 2 presenting the underlying valve positions, times and temperatures of the columns. For the according valve tags, compare with Figure 1. The step sequences are comparable with a TCAP process [17], but extended by the extraction from the second active separation column.

Table 2. Overview of the process steps for variant A automated by time-triggered valve actions. X refers to closed valves, O to opened valves. Process steps marked with OC refer to open cycles, meaning matter transfer across the system border, while CC marks closed cycles. Thermofluid temperatures set as boundary conditions for each column are given as C ("cold") and H ("hot"). For the given valve tags, refer to Figure 1.

Step	V-Exch	V-Pd	V-TiMn	V-Feed	T_{Pd}	T_{TiMn}	Time
1—OC	X	X	X	O	C	H	t_{feed}
2—CC	O	X	X	X	C	H	t_{exch}
3—CC	X	X	X	X	H	C	t_{heat}
4—CC	O	X	X	X	H	C	t_{exch}
5—CC	X	X	X	X	C	H	t_{heat}
6—CC	O	X	X	X	C	H	t_{exch}
7—CC	X	X	X	X	H	C	t_{heat}
8—OC	X	O	X	X	H	C	$t_{extr,Pd}$
9—CC	O	X	X	X	H	C	t_{exch}
10—CC	X	X	X	X	C	H	t_{heat}
11—OC	X	X	O	X	C	H	$t_{extr,TiMn}$

Variant B: The TSA process presented here, which is extended by a second active separation column, offers another operation mode, as both materials have the functionality of pumping. Instead of changing the absorption and desorption phases of the columns separately, the exchange valve is left permanently open. Operating this way lowers the

establishing process pressures and reduces pressure peaks, as the emerging hydrogen is not accumulated in an expand volume, and thus in the gas phase, but is immediately absorbed in the partner column, which is in the absorption phase. This means that during the temperature changes the columns continuously interact with each other, leading to a permanent gas flow between them. This operation mode takes advantage of the gas chromatographic effect, which is found to be more distinct than the thermodynamic separation effect caused by the isotopic preference during hydride formation [16]. Since the interacting columns pump each other due to their opposite process phases, lower process temperatures are needed to release the absorbed isotope species. Consequently, the establishing process pressures, which are linked to the process temperatures, are lowered, too. Operating the process with a permanently opened transfer valve reduces the necessary times for gas exchange and allows for complete fillings of both columns as no expand volume is needed. Furthermore, the process control and step automation is simplified and the necessary process equipment (like the transfer valve) is reduced. Higher sorption material amounts allow for higher gas throughputs and therefore reduce the number of parallel column systems. The according process step sequences for this process variant B is given in Table 3. However, less separation efficiency is to be expected. To examine if the presented operation mode fulfills the required separation task for the EU-DEMO IRPR system, the presented TSA model is used to perform simulations for a representative system scale and relevant process operation parameters (c.f. Section 3).

Table 3. Overview of the process steps for variant B automated by time-triggered valve actions for the modified process operation. X refers to closed valves, O to opened valves. Process steps marked with OC refer to open cycles, meaning matter transfer across the system border, while CC marks closed cycles. Thermofluid temperatures set as boundary conditions for each column are given as C ("cold") and H ("hot"). For the given valve tags, refer to Figure 1.

Step	V-Exch	V-Pd	V-TiMn	V-Feed	T_{Pd}	T_{TiMn}	Time
1—OC	O	X	X	O	C	H	t_{feed}
2—CC	O	X	X	X	H	C	$t_{heat} + t_{exch}$
3—CC	O	X	X	X	C	H	$t_{heat} + t_{exch}$
4—CC	O	X	X	X	H	C	t_{heat}
5—OC	O	O	X	X	H	C	$t_{extr,Pd}$
6—CC	O	X	X	X	C	H	$t_{exch} + t_{heat}$
7—OC	O	X	O	X	C	H	$t_{extr,TiMn}$

3. Simulation Results

An example simulation case is set up to demonstrate the utility of the presented model as a design and evaluation tool for the TSA process and to verify the assumptions made for TSA technology. Parameters are chosen to represent a relevant design and a realistic operation scenario. In addition, the investigation focuses on the operation variant B (c.f. Table 3), thus a permanent gas exchange between the separation columns. The objective is to evaluate whether the calculated enrichments in the product fractions identify this operation mode to be suitable for the requested separation task of the IRPR system.

For the preliminary column geometry dimensions, several design aspects were considered. Since the length of the column is the main influencing factor for the reachable product purification, 8 m is chosen to promote the chromatographic effect. The total sorption capacity and operational throughput is adjusted by the column diameter as it limits the amount of material that can be filled into the column. A trade-off between maximized column filling and tolerable heat transfer limitation for increasing diameters has to be made, which is why the column diameter is set to 10 mm. Based on the bulk densities of the investigated

absorption materials, this results in a molar absorption material amount of 2.4 mol in each column, assuming an ideal bed of spheres. The chosen process times and temperatures are based on preliminary experiments and simulations. Material characteristics like the equilibrium pressures and sorption kinetics are obtained from material pre-investigations. The resulting operation and design parameters for the example case are summarized in Table 4, along with the initialization parameters.

Table 4. Process and Design parameters used for demonstration of the TSA case and initialization values.

Parameter	Value	Unit
Geometry		
Column length L	8	m
Column diameter D_{col}	0.01	m
Particle diameter d_{p}	0.001	m
Material amount per column N_{mat}	2.4	mol
Process step times		
t_{exch}	100	s
t_{heat}	400	s
$t_{\mathrm{extr,Pd}} = t_{\mathrm{extr,TiMn}}$	120	s
t_{feed}	120	s
Feed composition and flow rates		
$\dot{N}_{\mathrm{feed}}$	8.1×10^{-4}	$\mathrm{mol\,s^{-1}}$
$z^{\mathrm{G}}_{\mathrm{feed},i}$	$H_2 = 0.01$	-
	$D_2 = T_2 = 0.245$	-
	DT = 0.49	-
$\dot{N}_{\mathrm{extr,Pd}} = \dot{N}_{\mathrm{extr,TiMn}}$	$0.5 \cdot \dot{N}_{\mathrm{feed}}$	$\mathrm{mol\,s^{-1}}$
Process temperatures and further parameters		
T_{hot}	Pd: 403	K
	TiMn: 333	K
T_{cold}	Pd: 283	K
	TiMn: 273	K
k_{heat}	50	$\mathrm{W m K^{-1}}$
k_{p}	3.5×10^{7} *	$\mathrm{s Pa^2 K^{-1.668} mol^{-1} m^{-1}}$
Δh_{sorb}	Pd: −31,925, TiMn: −35,665	$\mathrm{J mol^{-1}}$
k_{sorb}	5×10^{-6} **	$\mathrm{mol\,s^{-1} Pa^{-1}}$
$c^{\mathrm{S}}_{\mathrm{p}}$	500	$\mathrm{J kg^{-1} K^{-1}}$
`hys` (Desorption)	Pd: 0.71, TiMn: 0.83	-
Initialization		
$z^{\mathrm{S}}_{j,\mathrm{init,Pd}} = z^{\mathrm{S}}_{j,\mathrm{init,TiMn}}$	D = T = 0.495	-
	H = 0.01	-
$z^{\mathrm{G}}_{i,\mathrm{init,Pd}} = z^{\mathrm{G}}_{i,\mathrm{init,TiMn}}$	DT = 1	-
Pd Column		
c	0.65	$\mathrm{mol_Q mol_{mat}^{-1}}$
p	1.4×10^{5}	Pa
T	283	K
TiMn Column		
c	0.15	$\mathrm{mol_Q mol_{mat}^{-1}}$
p	1.2×10^{5}	Pa
T	333	K

* Derived by experiments described in Appendix A. ** Temperature dependence of reaction coefficient currently not implemented, but can be adjusted in the model in future if found necessary. A similar approach was chosen in [16].

The feed is configured to match the expected EU-DEMO compositions of 1% protium in an otherwise 50% D and 50% T mixture [2], and is set to refill an extracted amount of 10% of the complete system inventory. Equal amounts of product fractions are extracted from both columns to evaluate the obtainable enrichments in both separation columns. First, six closed loops in total reflux mode are simulated, as these are necessary to reach steady state conditions in the resulting compositions of isotopes. After these, open and closed cycles are alternated (c.f. Table 3).

The resulting temperature profiles (columns mid) for the simulated process cycles are shown in Figure 3. As can be seen, the selected heating and cooling times of 400 s are sufficient to reach the set temperatures for the absorption and desorption phase in both columns. Open cycles, i.e., gas transfer across the system boundary, have no impact on the temperature alteration. Since the transfer valve between the columns is permanently open, no significant temperature peak caused by the exothermic hydride formation is observable, as it would appear for a typical TSA process, where the hydrogen uptake is triggered by opening the transfer valve.

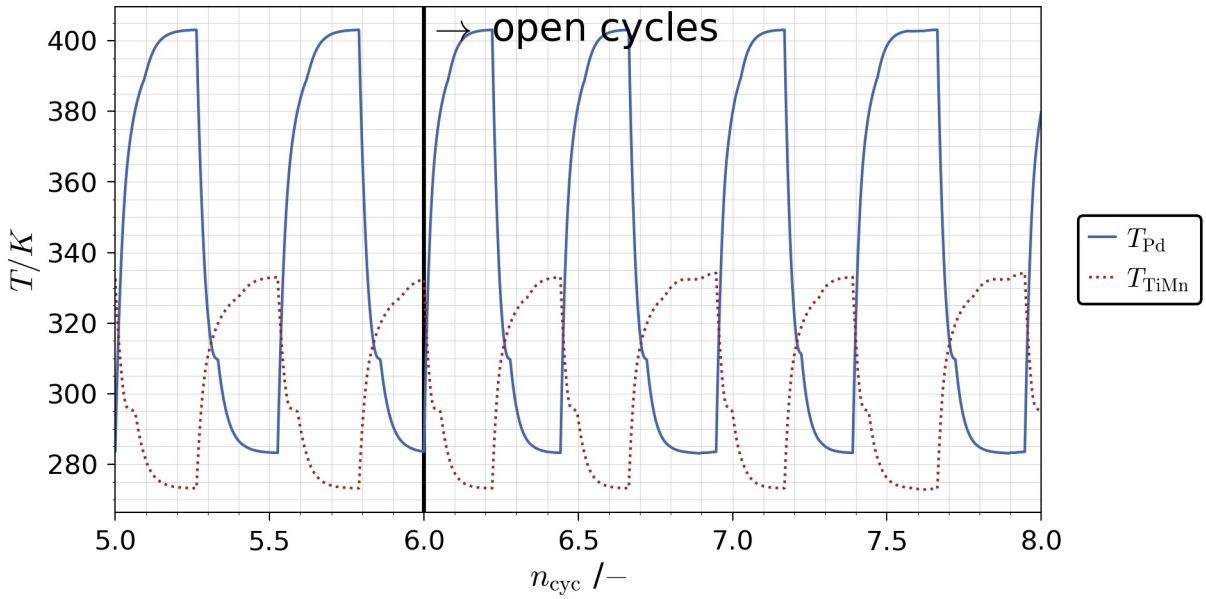

Figure 3. Simulated temperature profiles (columns mid) for palladium and TiMn columns, depending on the completed process cycle numbers. Open cycle operation follows at cycle number 6 after total reflux operation.

The corresponding process pressures at the end of each column are shown in Figure 4. Again, the computed data for the last closed cycle is given, followed by alternated open and closed cycles. For both scenarios, the resulting process pressures alternate between 100 and 2000 mbar. The highest or lowest pressure peaks occur at the ends of the columns, while the pressure at the exchange valve is always equal, as the valve offers negligible flow resistance compared to the column packing. Nevertheless, the given exchange times are sufficient to reach equilibration and full transfer of the gas between both columns. During open cycle operation, a product fraction of the palladium column can be extracted at 1400 mbar (TiMn column: 1200 mbar) at the beginning of extraction lowering to 600 mbar (TiMn column: 700 mbar) at extraction end. Similarly to the process temperatures, the establishing process pressures are not impacted by the switch from closed to open cycles.

The total in-process hydrogen inventory and its distribution between the columns during the process steps can be seen in Figure 5. Approximately 1 mol of isotopologues are treated within the given columns set-up. They are continuously transferred between the

separation columns depending on the phase (absorption or desorption). More than 95% of the entire inventory is absorbed in the materials, as the molar amount of hydrogen in the solid phase equals the total inventory of each column. During exchange, approximately 90% of the inventory in the palladium column is transferred to the TiMn column, while 80% is transferred in the opposite direction during exchange. The total inventory is reduced by 10% due to extraction from both columns and topped-up correspondingly by the feed stream. With this, a time-averaged throughput of 4.3×10^{-5} mols^{-1} is achieved, which corresponds to 0.1 Pam^{3}s^{-1} per column pair. For a process scale-up to the throughput of an EU-DEMO IRPR system, the simulated column pair has to be multiplied to a sufficient number.

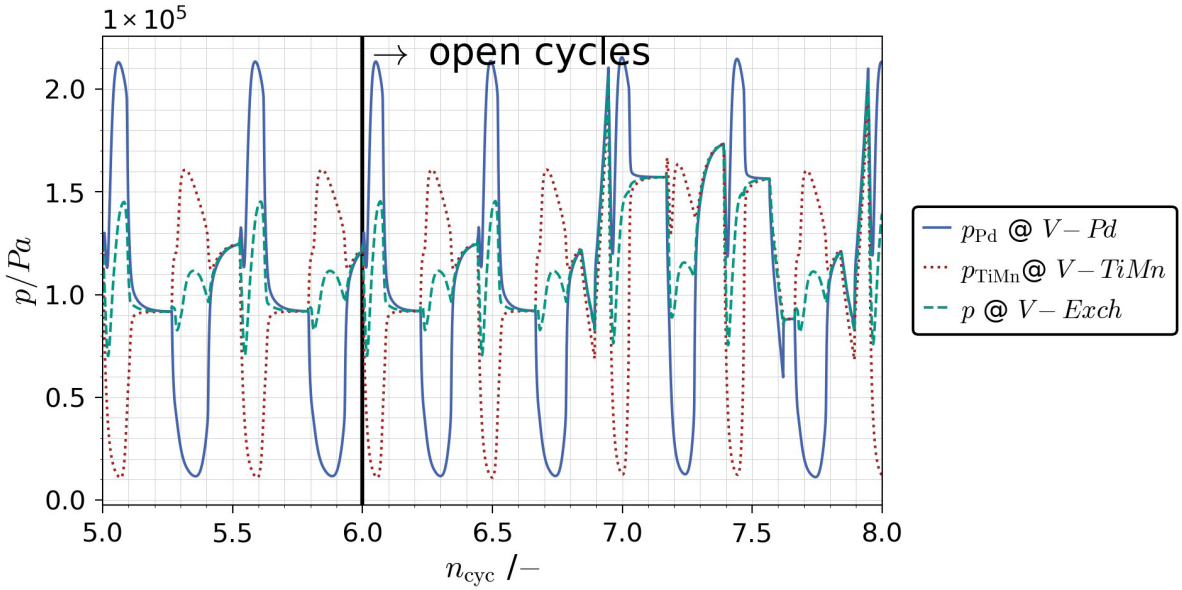

Figure 4. Simulated pressure profiles for palladium and TiMn at the extraction ports and at the exchange valve in dependence of the completed process cycle numbers. Open cycle operation follows at cycle number 6 after total reflux operation.

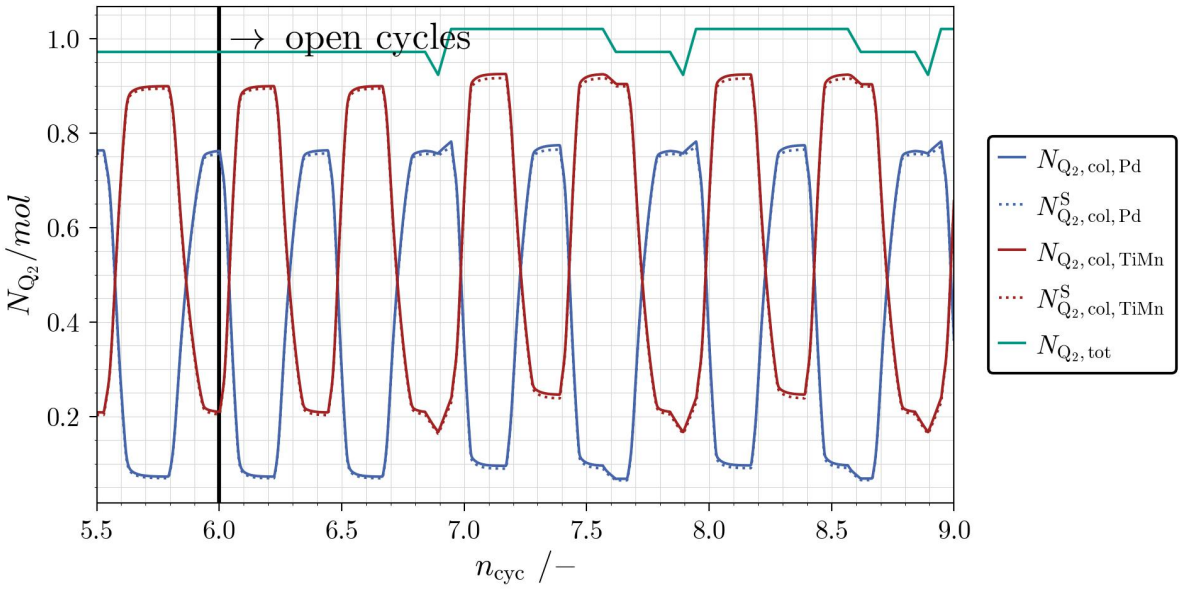

Figure 5. Isotopic molar inventories in the palladium and TiMn column, depending on the cycle number.

To evaluate the separation efficiency of both active columns, the establishing gas phase composition at the column ends (extraction valves) is plotted in Figure 6 (T_2 and D_2 molar fraction) and Figure 7 (molar fractions of remaining species). After six closed cycles, the

compositions in both columns reach a plateau, after which the operation is switched to include open cycles. After approximately four open cycles, the compositions re-establish to a new steady state. From this qualitative behavior two conclusions can be drawn: First, the improved TSA system exhibits typical operating characteristics, always reaching a stable operation point, enabling the operation of the IRPR system using TSA technology in principle. Second, after the extraction and re-feed within an open cycle, one exchange cycle between both columns is sufficient to maintain a constant product composition. This furthermore leads to fast cycling times and thus a maximized averaged system throughput, which underlines the process efficiency of the optimized TSA process.

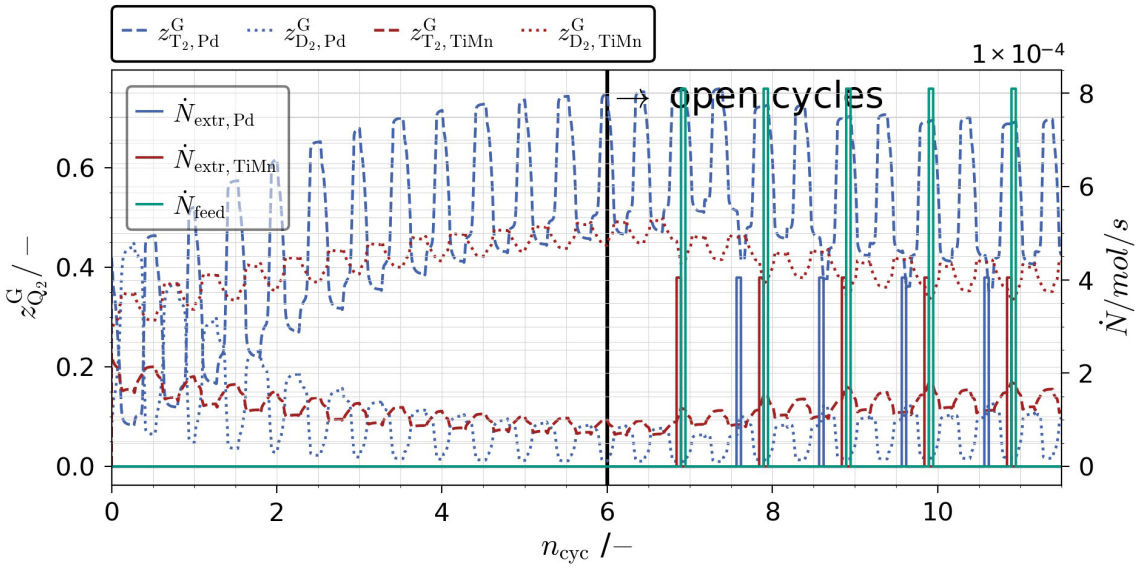

Figure 6. Establishing isotope compositions T_2 and D_2 at the extraction port of the palladium and TiMn columns, depending on the completed process cycles. At cycle number 6, the extraction of product fractions is tolerated.

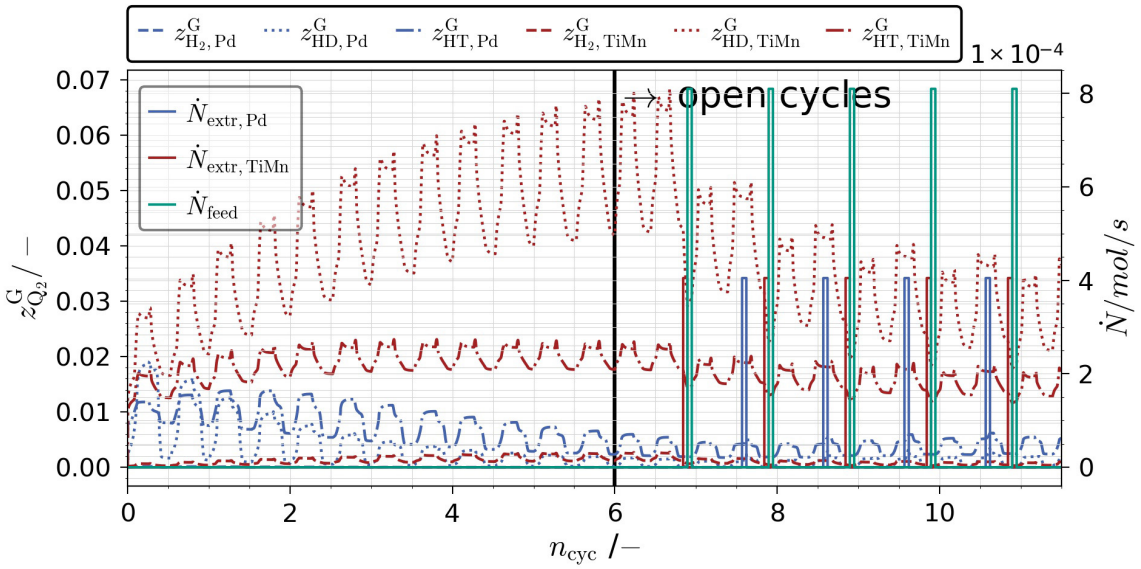

Figure 7. Establishing isotope compositions H_2, HD and HT at the extraction port of the palladium and TiMn columns, depending on the completed process cycles. At cycle number 6 the extraction of product fractions is tolerated.

From the species balance of the extracted products, it follows that the product stream of the palladium column is enriched by 30% in its T_2 content and depleted by 60% in

its H_2 content, relative to the treated feed. On the other hand, the product stream of the TiMn column is enriched by 67% in its H_2 content, while the T_2 is lowered by 20%. These enrichments achieved during one complete cycle in a steady state operation demonstrate the process efficiency and the promising potential of TSA for the IRPR system.

The presented results in this work follow from a representative example case. Nevertheless, the benefits of an improved TSA process utilizing two active separation columns and a modified operation mode (variant B), such as moderate operation pressures and temperatures, enhanced throughput and the corresponding reduced tritium inventory, can already be confirmed by the modeling results.

4. Summary and Outlook

To support the TSA process development for the EU-DEMO fuel cycle, a transient, rigorous TSA model was developed which is able to depict the process dynamics and automation. It enables the rapid evaluation of suitable process operation and design parameters. The TSA process is optimized by the utilization of a second active separation column filled with a titan–manganese alloy, showing an inverse isotope effect compared to palladium. This process extension enables an improved operation mode, which simplifies the process operation by reducing required valve operations, resulting in continuous gas exchange between both columns. It could be shown that this optimized TSA process allows for process operation at non-cryogenic temperatures and moderate process pressures below 2 bar(a) while reaching high throughputs, and thus proves TSA to be a promising semi-continuous separation technology able to fulfill the required IRPR system task within the EU-DEMO fuel cycle.

4.1. Future Work—Modeling

In future, the TSA model will be applied for the preliminary design of the EU-DEMO IRPR system. Further optimizations may include adapting the split factor between light and heavy products (adapted extraction amount ratios from the columns) to the required separation task and optimizing the column inventories and lengths.

4.2. Future Work—Experimental

A TSA mock-up in relevant EU-DEMO scale is planned as a facility within the fuel cycle demonstration platform DIPAK (DIR Integrated development platform Karlsruhe) currently under development at KIT. Separation experiments in this facility will be used to further validate the developed model at a relevant scale and define the optimal EU-DEMO IRPR design.

Author Contributions: Conceptualization, A.U., J.C.S. and T.G.; methodology, A.U. and J.C.S.; software, A.U. and J.C.S.; validation, A.U. and J.C.S.; formal analysis, A.U. and J.C.S.; investigation, A.U.; resources, T.G.; data curation, A.U.; writing—original draft preparation, A.U.; writing—review and editing, A.U. and J.C.S.; visualization, A.U.; supervision, S.H. and T.G.; project administration, S.H. and T.G.; funding acquisition, T.G. All authors have read and agreed to the published version of the manuscript.

Funding: This research is funded by the European Union via the Euratom Research and Training Programme (Grant Agreement No 101052200—EUROfusion).

Data Availability Statement: The original contributions presented in this study are included in the article. Further inquiries can be directed to the corresponding authors.

Acknowledgments: This work has been carried out within the framework of the EUROfusion Consortium, funded by the European Union via the Euratom Research and Training Programme (Grant Agreement No 101052200—EUROfusion). Views and opinions expressed are, however, those

of the author(s) only and do not necessarily reflect those of the European Union or the European Commission. Neither the European Union nor the European Commission can be held responsible for them. This work has been done under the Tritium-Matter Injection-Vacuum Programme of the EUROfusion DEMO Project. We acknowledge support by the KIT-Publication Fund of the Karlsruhe Institute of Technology. We gratefully thank M. Kind for his insightful discussions and valuable comments that greatly improved this manuscript.

Conflicts of Interest: The authors declare no conflicts of interest. The funders had no role in the design of the study; in the collection, analyses, or interpretation of data; in the writing of the manuscript; or in the decision to publish the results.

Abbreviations and List of Symbols

The following abbreviations and symbols are used in this manuscript:

Abbreviations

C1	Column 1 (Palladium)
C2	Column 2 (TiMn)
CC	Closed cycle
DIPAK	DIR Integrated Development Platform Karlsruhe
EU-DEMO	European Demonstration Fusion Power Plant
IRPR	Isotope Rebalancing and Protium Removal
KIT	Karlsruhe Institute of Technology
MFC	Mass flow controller
OC	Open cycle
PCI	Pressure concentration isotherm
PFR	Plug flow reverser
TCAP	Thermal Cycling Absorption Process
TSA	Temperature Swing Absorption

Symbol	*Description*	*Unit*
Latin symbols		
A	area	m^2
a	stoichiometric reaction coefficient	–
A_{jk}	correlation parameter (isotopic exchange)	–
B_{jk}	correlation parameter (isotopic exchange)	K
b	stoichiometric reaction coefficient	–
c	atomic hydrogen concentration in material	$\mathrm{mol_Q\,(mol_{mat})^{-1}}$
c_p	isobaric heat capacity	$\mathrm{J\,(mol\,K)^{-1}}$
D	diameter	m
H	enthalpy	J
h	specific enthalpy	$\mathrm{J\,(mol)^{-1}}$
hys	hysteresis factor	–
k	permeation parameter	m^2
K_{jk}	equilibrium constant (isotope exchange)	–
k_sorb	reaction coefficient	$\mathrm{mol\,(s\,Pa)^{-1}}$
k_CV	flow coefficient	$\mathrm{mol\,(s\,Pa)^{-1}}$
k_heat	heat-transfer coefficient	$\mathrm{J\,(m\,K)^{-1}}$
k_p	transport parameter	$\mathrm{(s\,Pa^2)\,(K^{1.668}\,mol\,m)^{-1}}$
L	length	m
m	mass	kg
N	molar amount	mol
$\dot{N}$	molar stream	$\mathrm{mol\,(s)^{-1}}$
p	pressure	Pa
$\dot{Q}$	heat flow	$\mathrm{J\,(m)^{-1}}$
R	ideal-gas constant	$\mathrm{J\,(mol\,K)^{-1}}$

$\dot{S}$	molar absorption/desorption stream	$\mathrm{mol\,(s)^{-1}}$
T	temperature	K
t	time	s
u	velocity	$\mathrm{m\,(s)^{-1}}$
x	position	m
z	molar fraction	–
Greek symbols		
μ	viscosity	Pa s
ρ	density	$\mathrm{kg\,(m^3)^{-1}}$
Subscripts		
col	column	
cold	cold temperature	
corr	correction	
exch	exchange	
extr	extraction	
feed	feed	
hot	hot temperature	
i	Isotopologue species Q_2: H_2, HD, HT, D_2, DT, T_2	
in	inlet	
init	initialization	
j,k,l	atomic Q-species: H, D, T	
mat	material	
oil	oil	
out	outlet	
sorb	absorption (sorption)	
r	reaction	
tot	total	
Superscripts		
eq	equilibrium	
G	gas phase	
pseudo	pseudo-molecular transition phase	
S	solid phase	
*	standard state	

Appendix A. Implementation and Validation of Flow Coefficient

To estimate a physically reliable value for the flow coefficient k_p, permeation experiments using H_2 were carried out in a column mock-up of relevant scale. Therefore, palladium was filled in a column of 1 m length and an inner diameter of 6 mm. The column was perfused at various feed streams and three temperatures to measure the pressure drop over the column's length at a saturated metal hydride and steady state. A flow sheet of the experiment is shown in Figure A1.

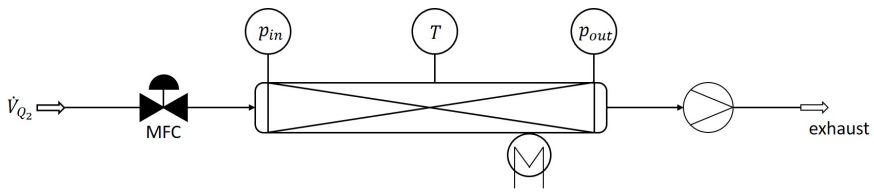

Figure A1. Flow sheet of experimental set-up for determination and verification of the permeation coefficient k_p.

k_p follows from the slope of the obtained pressure drops at room temperature over the utilized feed streams. As the Darcy equation is valid for small pressure drops a correction

was used for the evaluation of the data, as reported by Santomaso et al. for the pressure drops $p_{in} - p_{out}$ of elongated packed beds of the length L_{col} [25]:

$$\left(\frac{p_{in} - p_{out}}{L_{col}}\right)_{corr} = \frac{p_{in}^2 - p_{out}^2}{2p_{in}L_{col}} \quad \text{(A1)}$$

As standard gas viscosity, $\mu^*_{H_2}(293\ K) = 8.8 \times 10^{-6}$ Pas was used from the NIST database [26]. The measurements revealed a value of 3.5×10^7 $sPa^2K^{-1.668}mol^{-1}m^{-1}$ for k_p. Using this parameter and Equation (4), the estimated pressure drops over the column for the mock-up geometry (L_{col} = 1.05 m and D_{col} = 0.006 m) and for three relevant operation temperatures (T = room temperature, 50 and 100 °C) were simulated and compared with the experimental data. The results, showing a good agreement of experiment and simulation, can be seen in Figure A2.

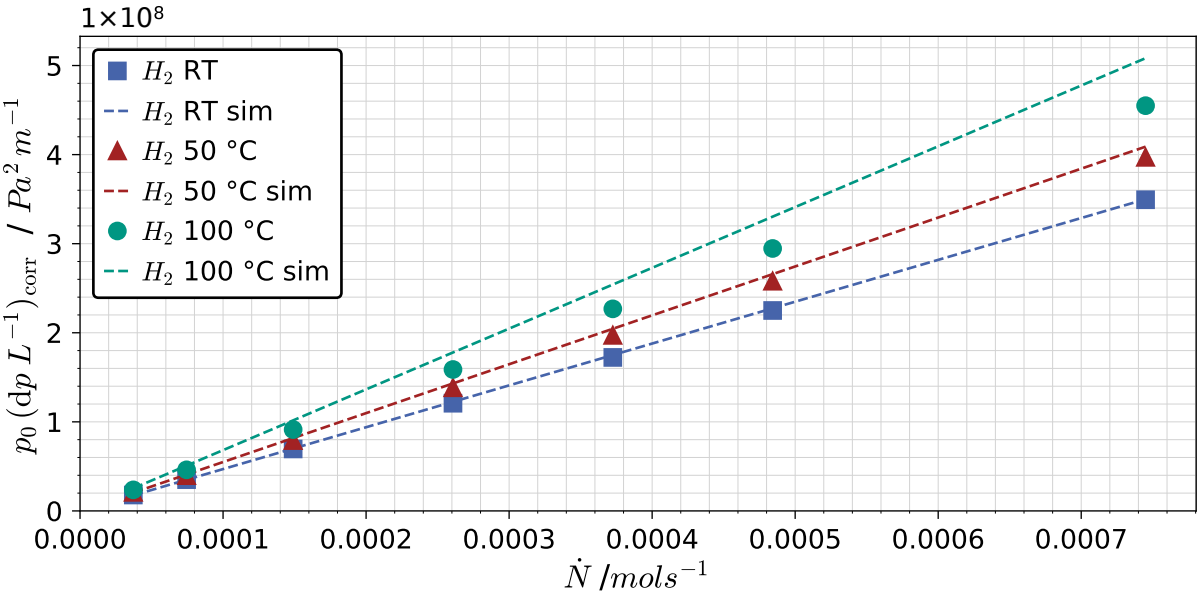

Figure A2. Comparison of measured and simulated pressure drops using k_p within the transport model for room temperature, 50 and 100 °C. Error bars are smaller than the markers.

Simulated pressure drops at room temperature vary in the range of 1 to 1.5% when compared to experimental data. Larger deviations are observed for increasing system temperature and increasing flows. Since the highest difference is ~12% at 100 °C, the deviation is considered tolerable.

References

1. Day, C.; Butler, B.; Giegerich, T.; Ploeckl, B.; Varoutis, S. A smart three-loop fuel cycle architecture for DEMO. *Fusion Eng. Des.* **2019**, *146*, 2462–2468. [CrossRef]
2. Day, C.; Battes, K.; Butler, B.; Davies, S.; Farina, L.; Frattolillo, A.; George, R.; Giegerich, T.; Hanke, S.; Härtl, T.; et al. The pre-concept design of the DEMO tritium, matter injection and vacuum systems. *Fusion Eng. Des.* **2022**, *179*, 113139. [CrossRef]
3. Xiao, X.; Sessions, H.T.; Rabun, R. Advanced Isotope Separation Technology for Fusion Fuel. *Fusion Sci. Technol.* **2022**, *78*, 253–257. [CrossRef]
4. Lässer, R. Palladium-tritium system. *Phys. Rev. B* **1982**, *26*, 3517–3519. [CrossRef]
5. Lässer, R.; Meuffels, P.; Feenstra, R. *Data Basis of the Solubilities of the Hydrogen Isotopes Protium (H), Deuterium (D) and Tritium (T) in the Metals V, Nb, Ta, Pd and in the Alloys* $V_{1-x}Nb_x$, $V_{1-x}Ta_x$, $Nb_{1-x}Mo_x$, $Pd_{1-x}Ag_x$; Jülich Report Documenting Solubility Data for H, D and T in Selected Metals and Alloys; Kernforschungsanlage Juelich GmbH: Jülich, Germany , 1988.
6. Scogin, J.H.; Poore, A.S. Startup and Operation of a Metal Hydride Based Isotope Separation Process. *Fusion Technol.* **1995**, *28*, 736–741. [CrossRef]

7. Lee, M.W. Tritium Separation Using Metal Hydrides. 2001. Available online: https://www.osti.gov/biblio/780496 (accessed on 16 November 2025).
8. Heung, L.K.; Sessions, H.T.; Poore, A.S.; Jacobs, W.D.; Williams, C.S. Next-Generation TCAP Hydrogen Isotope Separation Process. *Fusion Sci. Technol.* **2008**, *54*, 399–402. [CrossRef]
9. Xiao, X.; Heung, L.K.; Sessions, H.T. Recent Advances in SRS on Hydrogen Isotope Separation Using Thermal Cycling Absorption Process. *Fusion Sci. Technol.* **2015**, *67*, 643–646. [CrossRef]
10. Heung, L.K.; Sessions, H.T.; Xiao, X. TCAP hydrogen isotope separation using palladium and inverse columns. *Fusion Sci. Technol.* **2011**, *60*, 1331–1334. [CrossRef]
11. McDonald, K.D.; Malone, C.; Cooper, J.J.; Thompson, A.B.; Larsen, G.K. Benchmarking Hydrogen Isotope Separation Efficiency of Pd/k–Packed TCAP Columns. *Fusion Sci. Technol.* **2023**, *80*, 137–142. [CrossRef]
12. Neugebauer, C.; Hörstensmeyer, Y.; Day, C. Technology development for isotope rebalancing and protium removal in the EU-DEMO fuel cycle. *Fusion Sci. Technol.* **2020**, *76*, 215–220. [CrossRef]
13. Horen, A.S.; Lee, M.W. Metal Hydride Based Isotope Separation—Large-Scale Operations. *Fusion Technol.* **1992**, *21*, 282–286. [CrossRef]
14. Arias, A.A.; Schmierer, E.N.; Gettemy, D.; Howard, D.W.; Wermer, J.R.; Tuggle, D.G. Thermal Cycling Absorption Process (TCAP): Instrument and Simulation Development Status at Los Alamos National Laboratory. *Fusion Sci. Technol.* **2005**, *48*, 159–162. [CrossRef]
15. Ducret, D.; Ballanger, A.; Steimetz, J.; Laquerbe, C.; Baudouin, O.; Peyrigain, P. Hydrogen isotopes separation by thermal cycling absorption process. *Fusion Eng. Des.* **2001**, *58–59*, 417–421. [CrossRef]
16. Robinson, D.B.; Salloum, M. Comparison of designs of hydrogen isotope separation columns by numerical modeling. *Ind. Eng. Chem. Res.* **2023**, *62*, 3647–3658. [CrossRef]
17. Zhou, J.; Zhang, X.; Hao, S.; Huang, W. Dynamic simulation of Thermal Cycling Absorption Process with twin columns for hydrogen isotopes separation. *Int. J. Hydrogen Energy* **2014**, *39*, 13873–13879. [CrossRef]
18. Yan, Y.; Li, F.; Deng, L.; Wang, M.; Tang, T.; Fang, M.; Zhu, H.; Ye, X.; Chen, C. A fresh look at thermal cycling absorption process for hydrogen isotopes separation by dynamic simulation: Initial feeding process and total reflux mode. *Int. J. Hydrogen Energy* **2023**, *48*, 23894–23908. [CrossRef]
19. Schwenzer, J.C. A Process Simulator for the Prediction and Optimization of the Operation of the Fuel Cycle of a Fusion Power Plant. Doctoral Dissertation, Karlsruhe Institute of Technology (KIT), Karlsruhe, Germany, 2024. [CrossRef]
20. Flanagan, T.B.; Clewley, J. Hysteresis in metal hydrides. *J. Less Common Met.* **1982**, *83*, 127–141. [CrossRef]
21. Peters, B.J. Development of a Hydrogen-Selective Vacuum Pump on the Basis of Superpermeation = Entwicklung Einer auf Superpermeation Basierenden, Wasserstoffselektiven Vakuumpumpe. Ph.D. Dissertation, Karlsruhe Institute of Technology (KIT), Karlsruhe, Germany, 2020. [CrossRef]
22. Urey, H.C. The thermodynamic properties of isotopic substances. *J. Chem. Soc. (Resumed)* **1947**, 562–582. [CrossRef]
23. Charton, S.; Corriou, J.P.; Schweich, D. Modeling of hydrogen isotopes separation in a metal hydride bed. *Chem. Eng. Sci.* **1999**, *54*, 103–113. [CrossRef]
24. Wicke, E.; Nernst, G.H. Zustandsdiagramm und thermodynamisches Verhalten der Systeme Pd/H_2 und Pd/D_2 bei normalen Temperaturen; H/D-Trenneffekte. *Berichte Bunsenges. Phys. Chem.* **1964**, *68*, 224–235. [CrossRef]
25. Santomaso, A.C.; Carazzai, E.; Volpato, S. Particle size characterization through bed permeability tests. *Chem. Eng. Trans.* **2023**, *100*, 139–144. [CrossRef]
26. Muzny, C.D.; Huber, M.L.; Kazakov, A.F. Correlation for the viscosity of normal hydrogen obtained from symbolic regression. *J. Chem. Eng. Data* **2013**, *58*, 969–979. [CrossRef]